Computer Modeling in Engineering & Sciences CMES, vol.122, no.3, pp.1015-1038, 2020

An Equivalent Strain Based Multi-Scale Damage Model of Concrete

Shixue Liang[1, *] and Hankun Liu[2]

Abstract: A multi-scale damage model of concrete is proposed based on the concept of energy equivalent strain for generic two- or three-dimensional applications. Continuum damage mechanics serves as the framework to describe the basic damage variables, namely the tensile and compressive damage. The homogenized Helmholtz free energy is introduced as the bridge to link the micro-cell and macroscopic material. The crack propagation in micro-cells is modeled, and the Helmholtz free energy in the cracked micro-structure is calculated and employed to extract the damage evolution functions in the macroscopic material. Based on the damage energy release rates and damage consistent condition, the energy equivalent strain is used to expand the uniaxial damage model to the multi-dimensional damage model. Agreements with existing experimental data that include uniaxial tensile and compressive tests, biaxial compression and biaxial peak stress envelop demonstrate the capacity of the multi-scale damage model in reproducing the typical nonlinear performances of concrete specimens. The simulation of precast laminated concrete slab further demonstrates its application to concrete structures.

Keywords: Concrete, multi-scale, damage, energy equivalent strain.

1 Introduction

In the past decades, several continuum damage models [Faria, Oliver and Cervera (1998); Ju (1989); Krajcinovic and Silva (1982); Mazars and Pijaudier-Cabot (1989); Simo and Ju (1987); Wu, Li and Faria (2006)] were developed based on the continuum damage mechanics (CDM) framework. The continuum damage models have been applied to various engineering problems [Feng, Ren and Li (2018); Feng and Li (2015)], whereas the damage laws are somehow empirical. It is widely accepted that the damage of concrete is related to its complex microstructural behaviors, resulting from the development of micro-cracks and intrinsic interaction between cracking and plasticity. Therefore, the multi-scale modeling approach has been introduced to link the microscopic cracking process and the corresponding macroscopic damage law. Based on multi-scale modeling, the macroscopic constitutive equations are usually defined under the CDM

[1] School of Civil Engineering and Architecture, Zhejiang Sci-Tech University, Hangzhou, 310018, China.

[2] Sichuan Institute of Building Research, Chengdu, 610081, China.

[*] Corresponding Author: Liang Shixue. Email: liangsx@zstu.edu.cn.

Received: 30 June 2019; Accepted: 23 August 2019.

framework, while the damage variables and damage laws are obtained from the simulation of microstructures.

Stemming from the fundamental work of representative volume element (RVE) and homogenization [Hill (1984)], a number of multi-scale damage models [Bosco, Kouznetsova and Geers (2015); Dascalu, Bilbie and Agiasofitou (2008); Fish, Yu and Shek (1999); Sun and Li (2015)] had been brought by homogenization approach, among which the damage laws are particularly essential since they provide reliable descriptions of overall material degradation caused by the development of micro-defects. In order to simplify the homogenization process, Helmholtz free energy (HFE) bridging [Ren, Chen, Li et al. (2011)] was introduced to link the macro- and microscopic material properties for quasi-brittle material, such as concrete and rock. Chen et al. [Liang, Chen, Li et al. (2017); Lin, Chen and Liang (2016)] thoroughly studied the properties of the multi-scale damage model and evaluated the macrosopic concrete mechanical properties and microscopic random variations. Admittedly, these models incorporated the uniaxial multi-scale damage law into the CDM framework. Nevertheless, under the multi-dimensional loading conditions, it is numerically expensive to perform micro-cell analysis for all the stress states to attain the damage evolution. As a consequence, the damage evolution laws from uniaxial load in the aforementioned papers limit the application of the multi-scale damage model in the non-linear analysis of concrete structures, where most structural members are under multi-dimensional stresses.

In this paper, we are aiming at providing a multi-scale damage model of concrete which is applicable for multi-dimensional stress states. The paper is organized as follows. In Section 2, we consider the energy release rate based plastic damage model as the continuum damage framework. Two scalar damage variables, namely the tensile and compressive damage, are introduced, and each of them related to the basic degradation mechanisms of tension and shear. The decomposition of the effective stress enables us to define elastic HFE. The evolution law for plastic strains describes the plastic HFE, by which the total HEF and damage energy release rate can be acquired. In Section 3, the damage evolution law of the concrete is developed by the homogenization method and the multi-scale energy bridging from the micro-cell analysis. In Section 4, we apply the energy equivalent strain to bridge the gap between the damage law from the uniaxial micro-cell analysis and multi-dimensional damage model. Section 5 is devoted to the generation of micro-cell of concrete, in which the random distribution of multi-phases such as aggregates and mortar is represented by the two-phase random field. The cohesive crack model is considered as the tool in the micro-cell simulation, due to the highly nonlinear and discontinuous performance in the cracking process. In Section 6, the predictive capabilities of the model are assessed by means of numerical simulations, including the numerical verification on uniaxial tensile and compression tests, biaxial tests, biaxial peak stress and reinforced laminated concrete slab. Agreements between the numerical and the experimental results not only verify the proposed model but also reveal its application to two and three dimensions.

2 Continuum damage framework

2.1 Decomposition of effective stress

In CDM, concrete is considered as a homogeneous material, whereas the stiffness degradation caused by the micro-cracks are represented by a series of damage variables. In this case, proper damage variables that meet the experimental observation should be selected firstly. It is widely accepted that the degradation of concrete properties such as stiffness and strength are caused by tensile damage under tension. While under compression, there exist no tensile stress in the deviatoric space, the compressive failure of concrete is induced by the development of shear cracks rather than the compressive stress [Resende (1987)]. It is also observed that the strength of the concrete is increased greatly under triaxial compression due to the confinement of the shear cracks. Therefore, the damage is activated by the shear damage mechanism under compression [Resende (1987)].

Continuum damage mechanics is based on the thermodynamics of irreversible processes [Lubliner (1972)]. As the foundation of the constitutive model, the effective stress concept [Simo and Ju (1987)] serves as the extension of the "net area" assumption. The continuum effective stress $\bar{\boldsymbol{\sigma}}$ in the damaged material with the consideration of the elastoplastic behavior can be assumed as

$$\bar{\boldsymbol{\sigma}} = \boldsymbol{C}_0 : \boldsymbol{\varepsilon}^e = \boldsymbol{C}_0 : \left(\boldsymbol{\varepsilon} - \boldsymbol{\varepsilon}^p\right) \tag{1}$$

where $\boldsymbol{C}_0$ is the fourth-order isotropic linear-elastic stiffness; $\boldsymbol{\varepsilon}$, $\boldsymbol{\varepsilon}^e$ and $\boldsymbol{\varepsilon}^p$ indicate the total strain, elastic strain and plastic strain tensor, respectively.

In order to clearly distinguish stress contributions due to tension or compression, thereafter to produce independent tensile and compressive damage, the decomposition of the effective stresses [Faria, Oliver and Cervera (1998); Ortiz (1985); Wu, Li and Faria (2006)] are given in Eqs. (2) and (3) as

$$\bar{\boldsymbol{\sigma}}^+ = \boldsymbol{P}^+ : \bar{\boldsymbol{\sigma}} \tag{2}$$

$$\bar{\boldsymbol{\sigma}}^- = \bar{\boldsymbol{\sigma}} - \bar{\boldsymbol{\sigma}}^+ = \boldsymbol{P}^- : \bar{\boldsymbol{\sigma}} \tag{3}$$

where $\boldsymbol{P}^+$ and $\boldsymbol{P}^-$ are the fourth-order projection tensors. The expression of $\boldsymbol{P}^+$ and $\boldsymbol{P}^-$ [Faria, Oliver and Cervera (1998)] can be provided as

$$\boldsymbol{P}^+ = \sum_i H\left(\hat{\bar{\sigma}}_i\right)\left(\boldsymbol{p}_{ii} \otimes \boldsymbol{p}_{ii}\right) \tag{4}$$

$$\boldsymbol{P}^- = \boldsymbol{I} - \boldsymbol{P}^+ \tag{5}$$

where $\boldsymbol{I}$ is the fourth-order identity tensor; $H\left(\hat{\bar{\sigma}}_i\right)$ is the Heaviside function computed for the i -th eigenvalue $\hat{\bar{\sigma}}_i$.

And the second-order symmetric tensor $\boldsymbol{p}_{ij}$ is defined as

$$\boldsymbol{p}_{ij} = \boldsymbol{p}_{ji} = \frac{1}{2}\left(\boldsymbol{n}_i \otimes \boldsymbol{n}_j + \boldsymbol{n}_j \otimes \boldsymbol{n}_i\right) \tag{6}$$

where $\boldsymbol{n}_i$ is the i -th order normalized eigenvector corresponding to $\hat{\bar{\sigma}}_i$.

Substitute the effective stress of Eqs. (2) and (3) into the definition of HFE, the initial elastic HFE can be written as

$$\psi_0^e\left(\boldsymbol{\varepsilon}^e\right)=\frac{1}{2}\overline{\boldsymbol{\sigma}}:\boldsymbol{\varepsilon}^e=\frac{1}{2}\overline{\boldsymbol{\sigma}}^+:\boldsymbol{\varepsilon}^e+\frac{1}{2}\overline{\boldsymbol{\sigma}}^-:\boldsymbol{\varepsilon}^e=\psi_0^{e+}+\psi_0^{e-} \tag{7}$$

Considering the tensile and compressive damage definition, the damaged elastic HFE can be defined as

$$\psi^e\left(\boldsymbol{\varepsilon}^e,d^+,d^-\right)=\psi^{e+}\left(\boldsymbol{\varepsilon}^e,d^+\right)+\psi^{e-}\left(\boldsymbol{\varepsilon}^e,d^-\right) \tag{8}$$

where the corresponding ψ^{e+} and ψ^{e-} are defined as

$$\psi^{e\pm}\left(\boldsymbol{\varepsilon}^e,d^\pm\right)=\left(1-d^\pm\right)\psi_0^{e\pm} \tag{9}$$

2.2 Constitutive equations

For a constitutive law to be established, the total HFE potential can be defined as the sum of elastic HFE ψ^e and plastic HFE ψ^p as

$$\psi\left(\boldsymbol{\varepsilon}^e,\boldsymbol{\zeta},d^+,d^-\right)=\psi^e\left(\boldsymbol{\varepsilon}^e,d^+,d^-\right)+\psi^p\left(\boldsymbol{\varepsilon}^e,\boldsymbol{\zeta},d^+,d^-\right) \tag{10}$$

where $\boldsymbol{\zeta}$ denotes a set of plastic parameters.

Differentiating equation with respect to time, one gets

$$\dot{\psi}=\frac{\partial\psi^e}{\partial\boldsymbol{\varepsilon}^e}:\dot{\boldsymbol{\varepsilon}}^e+\frac{\partial\psi}{\partial d^+}\dot{d}^++\frac{\partial\psi}{\partial d^-}\dot{d}^-+\frac{\partial\psi^p}{\partial\boldsymbol{\zeta}}\cdot\dot{\boldsymbol{\zeta}} \tag{11}$$

According to the second principle of thermodynamics, for any purely isothermal mechanical process, the Clausius-Duheim inequality has to be fulfilled

$$\dot{\gamma}=-\dot{\psi}+\boldsymbol{\sigma}:\boldsymbol{\varepsilon}\geq 0 \tag{12}$$

The assumption that the damage and plastic unloading are irreversible processes is applied to represent the thermodynamic conditions as

$$\boldsymbol{\sigma}=\frac{\partial\psi^e}{\partial\boldsymbol{\varepsilon}^e} \tag{13}$$

$$\dot{\gamma}^d=-\left(\frac{\partial\psi}{\partial d^+}\dot{d}^++\frac{\partial\psi}{\partial d^-}\dot{d}^-\right)\geq 0 \tag{14}$$

$$\dot{\gamma}^p=\boldsymbol{\sigma}:\boldsymbol{\varepsilon}^p-\frac{\partial\psi^p}{\partial\boldsymbol{\zeta}}\cdot\boldsymbol{\zeta}\geq 0 \tag{15}$$

Substituting Eqs. (7)-(9) into Eq. (13), it yields

$$\boldsymbol{\sigma}=\frac{\partial\psi^e}{\partial\boldsymbol{\varepsilon}^e}=\left(1-d^+\right)\boldsymbol{P}^+:\overline{\boldsymbol{\sigma}}+\left(1-d^-\right)\boldsymbol{P}^-:\overline{\boldsymbol{\sigma}}=\left(\boldsymbol{I}-\boldsymbol{D}\right):\overline{\boldsymbol{\sigma}}=\left(\boldsymbol{I}-\boldsymbol{D}\right):\boldsymbol{C}_0:\left(\boldsymbol{\varepsilon}-\boldsymbol{\varepsilon}^p\right) \tag{16}$$

where $\boldsymbol{D}$ is the fourth order damage tensor with the expression $\boldsymbol{D}=\left(d^{+}\boldsymbol{P}^{+}+d^{-}\boldsymbol{P}^{-}\right)$. It can be seen in Eq. (16) that the evolution of both damage and plastic strain should be calculated for the integration of constitutive relationship.

By the observation of Eq. (16), the tensile and compressive damage energy release rates (DERRs) can be defined as Y^{+} and Y^{-} with the expressions as [Wu, Li and Faria (2006)]

$$Y^{+}=\frac{\partial\psi}{\partial d^{+}}=\sqrt{2E_0\psi_0^{+}}=\sqrt{E_0\left(\bar{\boldsymbol{\sigma}}^{+}:\boldsymbol{\Lambda}_0:\bar{\boldsymbol{\sigma}}\right)} \tag{17}$$

$$Y^{-}==\frac{\partial\psi}{\partial d^{+}}=\sqrt{\psi_0^{-}/b_0}=\varphi\bar{I}_1+\sqrt{3\bar{J}_2} \tag{18}$$

where $\boldsymbol{\Lambda}_0$ is the fourth-order compliance tensor; $\bar{I}_1$ is the first invariants of effective stress $\bar{\boldsymbol{\sigma}}$; $\bar{J}_2$ is the second invariants of $\bar{\boldsymbol{s}}$ (the deviatoric components of $\bar{\boldsymbol{\sigma}}$); b_0 is the material parameter. Parameter φ is related to the ratio between the yield strengths under equal-biaxial and uniaxial compression ϑ (usually taken as 1.16) as

$$\varphi=\frac{\vartheta-1}{2\vartheta-1} \tag{19}$$

According to the thermodynamical principles, consistent damage laws are based on $Y^{\pm}$ in a group of damage models and DERRs are considered as the conjugated forces to the damage variables.

2.3 Plastic strain evolution

Li et al. [Li and Ren (2009)] proposed a practical plastic evolution model with the coupling of plasticity and damage as

$$\boldsymbol{\varepsilon}^{p}=\boldsymbol{C}_0^{-1}:F\left(\boldsymbol{D}\right):\boldsymbol{C}_0:\boldsymbol{\varepsilon} \tag{20}$$

where $F\left(\boldsymbol{D}\right)$ is a forth-order tensor function of damage scalars and takes the form

$$F\left(\boldsymbol{D}\right)=f_p^{+}\left(d^{+}\right)\boldsymbol{P}^{+}+f_p^{-}\left(d^{-}\right)\boldsymbol{P}^{-} \tag{21}$$

A linear function of the function $f_p^{\pm}$ is adopted as

$$f_p^{\pm}\left(d^{\pm}\right)=\zeta_p^{\pm}d^{\pm} \tag{22}$$

The plastic parameter $\zeta_p^{\pm}$ matches the criteria

$$0\le\zeta_p^{\pm}\le 1 \tag{23}$$

Since the multi-scale damage representation is the main concern in this study, the empirical plastic strain evolution is applied for the simplicity of the model. The theoretical models such as "effective stress space plasticity" [Ju (1989)] can also be resorted to establish the evolution laws for the plastic strain.

3 Multi-scale damage representation

For the integrity of the constitutive law, evolution of the plastic strain has been formulated in Section 2.3, whereas the damage evolution should be determined to account for the degradation of the mechanical properties. Initiating from the development of the micro-defects (micro-cracks, micro-voids, etc.), the damage should be studied and investigated on micro-scale [Bazant and Planas (1997)].

3.1 Multi-scale energy bridging

Introduce $\boldsymbol{x}=(x_1,x_2)$ and $\boldsymbol{y}=(y_1,y_2)$ to indicate the macroscopic coordinate and the microscopic coordinate in a 2-D problem, the transformation between $\boldsymbol{x}$ and the $\boldsymbol{y}$ could be defined by a parameter λ as

$$\boldsymbol{x}=\frac{\boldsymbol{y}}{\lambda} \tag{24}$$

As depicted in Fig. 1, the domain Ω and the boundary Γ are considered on the macro-scale. Within the Ω, the micro-cell Ω_y contains a distribution of arbitrary micro-cracks. Γ_c indicates the sum of all the micro-void/crack surfaces. When it comes to the concrete, it is generally considered as a kind of a homogeneous material on macro-scale, which is demonstrated as domain Ω. However, the randomly distributed heterogeneities in concrete micro-structures (aggregates, cement, etc.) and defects (micro-cracks and micro-voids) are too big to neglect comparing to micro-cell sizes. Thus, we consider the micro-cell as a heterogeneous material with micro-cracks in it. It is believed that the micro-cell should contain sufficient microscopic information and its size should not be too small. As the foundation of multi-scale analysis, the representative volume element (RVE) and its properties [Hill (1984); Ostoja-Starzewski (2006)] are also considered in the present paper.

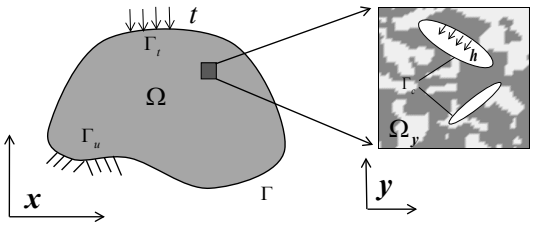

Figure 1: Macro structure and micro-cell

According to the aforementioned two-scale description of the material, the equilibrium equation without body forces and boundary conditions contain the information both on micro-scale and macro-scale as

$$\nabla\cdot\boldsymbol{\sigma}^{\lambda}=0 \text{ in } \Omega \tag{25}$$

$$\boldsymbol{\sigma}^{\lambda}\cdot\boldsymbol{n}=\boldsymbol{t} \text{ in } \Gamma_t \tag{26}$$

$$\boldsymbol{u}^{\lambda}=\overline{\boldsymbol{u}} \text{ in } \Gamma_u \tag{27}$$

$$\boldsymbol{\sigma}^{\lambda}\cdot\boldsymbol{n}=\boldsymbol{h}\ \text{ on }\ \Gamma_c \tag{28}$$

where $\boldsymbol{\sigma}^{\lambda}$ is the total stress; superscript "λ" is the total solution combines the coarse and fine scale; $\boldsymbol{n}$ is the surface normal vector; $\boldsymbol{u}^{\lambda}$ is the total displacement; $\bar{\boldsymbol{u}}$ is the prescribed displacement on the surface Γ_u; $\boldsymbol{t}$ is the surface traction on Γ_t and $\boldsymbol{h}$ is the surface traction on Γ_c.

Based on the homogeneous definition on macro-scale, the homogenized stress and stain are defined based on the tractions and displacements prescribed on the outer boundary of the micro-cell as follows

$$\boldsymbol{\sigma}=\frac{1}{V_y}\oint_{\partial\Omega_y}\left(\boldsymbol{t}^{\lambda}\otimes\boldsymbol{x}\right)\mathrm{d}\Omega \tag{29}$$

$$\boldsymbol{\varepsilon}=\frac{1}{2V_y}\oint_{\partial\Omega_y}\left(\boldsymbol{u}^{\lambda}\otimes\boldsymbol{n}+\boldsymbol{n}\otimes\boldsymbol{u}^{\lambda}\right)\mathrm{d}\Gamma \tag{30}$$

where V_y is the volume the micro-cell. Since concrete is considered as a homogeneous material in the CDM framework, the definition of homogenized stress and strain in Eqs. (29) and (30) is consistent with the definition of the stress and strain in CDM. The same notations $\boldsymbol{\sigma}$, $\boldsymbol{\varepsilon}$ are used both for the homogenized stress and strain herein and the stress and strain in CDM framework.

To consider the heterogeneities on micro-scale, we introduce the averaged stress and strain of a micro-cell as

$$\left\langle\boldsymbol{\sigma}^{\lambda}\right\rangle=\frac{1}{V_y}\int_{\Omega_y}\boldsymbol{\sigma}^{\lambda}\mathrm{d}\Omega \tag{31}$$

$$\left\langle\boldsymbol{\varepsilon}^{\lambda}\right\rangle=\frac{1}{V_y}\int_{\Omega_y}\boldsymbol{\varepsilon}^{\lambda}\mathrm{d}\Omega \tag{32}$$

Substituting Eq. (31) into Eq. (29), we can attain the relationship between the average stress and homogenized stress

$$\begin{aligned}\left\langle\boldsymbol{\sigma}^{\lambda}\right\rangle&=\frac{1}{V_y}\int_{\Omega_y}\boldsymbol{\sigma}^{\lambda}\mathrm{d}\Omega\\&=\boldsymbol{\sigma}-\frac{1}{V_y}\oint_{\Gamma_c}\left(\boldsymbol{t}^{\lambda}\otimes\boldsymbol{x}\right)\mathrm{d}\Gamma\\&=\boldsymbol{\sigma}\end{aligned} \tag{33}$$

Inserting Eq. (32) into Eq. (30), the relationship between average strain and homogenized strain is as follows:

$$\begin{aligned}\left\langle\boldsymbol{\varepsilon}^{\lambda}\right\rangle&=\frac{1}{V_y}\int_{\Omega_y}\boldsymbol{\varepsilon}^{\lambda}\mathrm{d}\Omega\\&=\boldsymbol{\varepsilon}-\frac{1}{2V_y}\times\oint_{\Gamma_c}\left(\boldsymbol{n}\otimes\boldsymbol{u}^{\lambda}+\boldsymbol{u}^{\lambda}\otimes\boldsymbol{n}\right)\mathrm{d}\Gamma\end{aligned} \tag{34}$$

With the micro-cracks in the domain, the homogenized strain contains two parts: the average strain which is the same as the elastic domain and the additional strain induced by the displacement discontinuity across the crack surfaces.

After the definition of homogenized and averaged stress and strain on macro- and micro-scale, a micro-crack informed damage representing framework [Ren, Chen, Li et al. (2011)] is adopted in this manuscript to obtain the macroscopic damage evolution from the cracked micro-cell. Taking the relationship between the homogenized and averaged stress and strain into the HFE definition, the multi-scale energy bridging [Ren, Chen, Li et al. (2011)] is given as (see Appendix A for detailed derivations based on the divergence theorem)

$$\begin{aligned}\psi^e &= \frac{1}{2}\boldsymbol{\sigma}:\boldsymbol{\varepsilon} \\ &= \frac{1}{V_y}\left(\int_{\Omega_y}\boldsymbol{\sigma}^\lambda:\varepsilon^\lambda \mathrm{d}\Omega+\frac{1}{2}\oint_{\Gamma_c}\boldsymbol{u}^\lambda\cdot\boldsymbol{h}\mathrm{d}\Gamma\right) \\ &= \frac{1}{V_y}\left(\int_{\Omega_y}\psi^\lambda \mathrm{d}\Omega+\frac{1}{2}\oint_{\Gamma_c}\boldsymbol{u}^\lambda\cdot\boldsymbol{h}\mathrm{d}\Gamma\right)\end{aligned} \tag{35}$$

As implied in Eq. (35) that the homogenized HFE is equal to sum of averaged HEF and the energy brought by the micro-cracks in a micro-cell.

Recalling the definition of the tensile and compressive damage in Eq. (9), we can rewrite the damage as

$$d^{\pm} = 1-\frac{\psi^{e\pm}}{\psi_0^{e\pm}} \tag{36}$$

In the application, the uniaxial tensile and shear loads, which represent the tensile and compressive damage correspondingly, can be applied to the micro-cell for the tensile and compressive damage evolution curves.

3.2 Tensile damage variable

As mentioned in Section 2.1, the micro-cell under uniaxial tension can be formulated to obtain the tensile damage evolution curve, in which $\psi_0^{e-}=0$, $d^-=0$. The uniaxial tension applied on the micro-cell is given in Fig. 2.

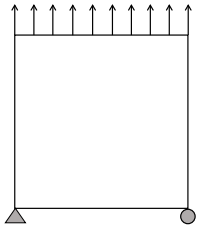

Figure 2: Uniaxial tension

The tensile damage can be expressed as

$$d^{+}=1-\frac{\psi^{e+}\left(\boldsymbol{\varepsilon}^{e}\right)}{\psi_{0}^{e+}} \tag{37}$$

where the tensile HFE ψ^{e+} is obtained by multi-scale energy bridging in Eq. (36), ψ_{0}^{e+} is the elastic tensile HFE.

3.3 Compressive damage variable

It is emphasized before that the compressive damage is actually brought about shear damage mechanics. Hence, in order to attain the compressive damage, the shear should be applied to the micro-cell. The micro-cell under pure shear can be formulated to obtain the shear damage evolution curve, in which $\psi_{0}^{-}=0$, $d^{-}=0$. The boundary condition of micro-cell is depicted in Fig. 3.

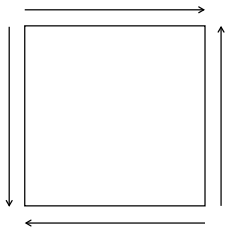

Figure 3: Pure shear

The shear damage can be expressed as

$$d_{s}=1-\frac{\psi^{e_s}\left(\boldsymbol{\varepsilon}^{e}\right)}{\psi_{0}^{e_s}} \tag{38}$$

where the shear HFE ψ^{e_s} is obtained by multi-scale energy bridging in equation, $\psi_{0}^{e_s}$ is the elastic shear HFE.

Noting that the shear damage d_s cannot be interpolated in Eqs. (9) and (37) as the compressive damage, a relationship between the compressive damage variable and shear damage variable should be established. Under uniaxial compression, the damage evolution caused by crack development in the micro-cell is shown in Fig. 4.

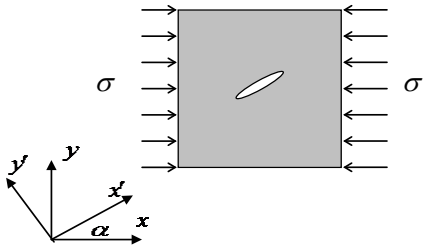

Figure 4: Crack under compression

Assuming that the angle between the compression and main crack is α, we can transform the coordinate xy to $x'y'$ as

$$\begin{cases} \sigma'_x = \sigma\cos^2\alpha \\ \sigma'_y = \sigma\sin^2\alpha \\ \tau' = (\sigma\sin 2\alpha)/2 \end{cases} \tag{39}$$

where σ'_x, σ'_y and τ' are the stresses in $x'y'$.

The corresponding normal strain is obtained as

$$\begin{cases} \varepsilon'_x = \dfrac{1}{E}[\sigma\cos^2\alpha - \nu\sigma\sin^2\alpha] \\ \varepsilon'_y = \dfrac{1}{E}[\sigma\sin^2\alpha - \nu\sigma\cos^2\alpha] \end{cases} \tag{40}$$

where ν is the Poisson's ratio.

While, the damage should be considered with shear strain as

$$\tau = (1-d_s)G\gamma \tag{41}$$

where G is the shear modulus.

Back to xy coordinate, it yields

$$\begin{aligned} \varepsilon &= \left(1-\frac{1+v}{2}\sin^2 2\alpha\right)\frac{\sigma}{E} + \left[\frac{1+v}{2\left(1-d^-\right)}\sin^2 2\alpha\right]\frac{\sigma}{E} \\ &= \left[1+\left(\frac{d^-}{1-d^-}\right)\frac{1+v}{2}\sin^2 2\alpha\right]\frac{\sigma}{E} \end{aligned} \tag{42}$$

Eq. (42) can be simplified as

$$\sigma = (1-d^-)E\varepsilon \tag{43}$$

$$d^- = \frac{(1-\beta)d_s}{1-\beta d_s} \tag{44}$$

$$\beta = 1-\frac{1+v}{2}\sin^2 2\alpha \tag{45}$$

With substitution the shear damage d_s into Eq. (44), the compressive damage can be attained.

4 Multi-dimensional damage law

Indeed, the most accurate way to obtain the damage under multi-dimensional stress state is the simulated strain-damage curve directly from the micro-cell analysis under the same stress-state. In other words, we can obtain exactly the same energy dissipation, which can be represented by the damage for each stress state from the micro-cell simulation rather

than introducing the simplification and empirical assumption. In the engineering problems, especially for the structures under multi-dimensional loads, it is difficult to perform micro-cell analysis for all the stress states to attain the damage evolution. Hence, in this section the energy equivalent strain is introduced to link the uniaxial damage law from micro-cell analysis to the multi-dimensional continuum damage model.

Under CDM framework, authors in this paper utilize the energy equivalent strain into the multi-scale damage model which can be considered as the expansion of the energy equivalent strain. A general form can be given to represent the relationship between the damage and DERRs as

$$d^{\pm} = g^{\pm}\left(Y^{\pm}\right) \tag{46}$$

Eq. (46) implies that the damage will be the same if the DERRs are the same, no matter the uniaxial or multi-axial loads are applied to the concrete. Eq. (46) is called damage consistent condition [Li and Ren (2009)].

Let us recall the DERRs in Eqs. (17) and (18) and rewrite them as

$$Y^{\pm} = Y^{\pm}\left(\bar{\boldsymbol{\sigma}}\right) = Y^{\pm}\left(\boldsymbol{\varepsilon}^{e}\right) = Y^{\pm}\left(\varepsilon_1^e, \varepsilon_2^e, \varepsilon_3^e\right) \tag{47}$$

Actually, for the uniaxial loading $\left(\sigma_2 = 0;\quad \sigma_3 = 0\right)$, Eq. (17) and are converted to

$$Y^{+} = E_0 \varepsilon^{e+} \tag{48}$$

$$Y^{-} = \left(\varphi - 1\right) E_0 \varepsilon^{e-} \tag{49}$$

Under the damage consistent condition, for any multi-axial stress state, there exists a uniaxial stress state that has the same DERRs as

$$Y^{\pm} = Y^{\pm}\left(\varepsilon_1^e, \varepsilon_2^e, \varepsilon_3^e\right) = Y^{\pm}\left(\varepsilon_q^e\right) \tag{50}$$

where ε_q^e is the energy equivalent strain.

Substituting Eqs. (48) and (49) into (50), we can address the expression of the energy equivalent strain as

$$\varepsilon_q^{e+} = \frac{Y^{+}}{E_0} \tag{51}$$

$$\varepsilon_q^{e-} = \frac{Y^{-}}{\left(\alpha - 1\right) E_0} \tag{52}$$

Replacing $\boldsymbol{\varepsilon}^{e}$ of tensile and shear given in Eqs. (37) and (38) by energy equivalent strain ε_q^{e+}, we can interpolate the uniaxial damage curve into the multi-dimensional CDM framework.

5 Micro-cell simulation approach

Under the multi-scale damage representation given in Section 3, the essential step in obtaining the damage evolution functions is the micro-cell analysis. In the present study, the cohesive element is adopted to model discontinuities in the cracking process. In order

to capture the heterogeneous micro-structure of concrete, fracture property (fracture energy) of the micro-cell is represented by the random field approach.

5.1 Random cohesive model

Since the initiation, development and coalescence of micro-cracks are highly irregular and random, the random cohesive model is generated to simulate the cracking process of concrete [Li and Siegmund (2004); Liang, Ren and Li (2018, 2012)]. As depicted in Fig. 5, each Delaunay triangle is directly modeled by a linear displacement based finite element, while zero-thickness cohesive elements are inserted between each finite element. Due to the strong nonlinearities introduced by the cracking process, we choose ABAQUS Explicit solution algorithm to get the integration of the cracking process. The numerical model of the uniaxial tensile micro-cell and its boundary conditions are given in Fig. 5. And the corresponding pure shear micro-cell can also be formulated by changing its boundary conditions.

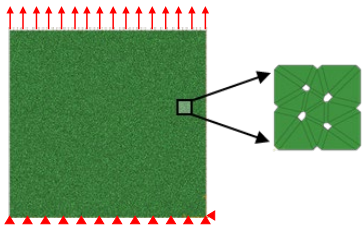

Figure 5: Numerical model of micro-cell

The fracture behaviors are described by the linear decay cohesive law (Fig. 6), with which the cohesion on the crack tips can be solely determined by the maximum cohesive stress f_t and the cohesive energy G_f.

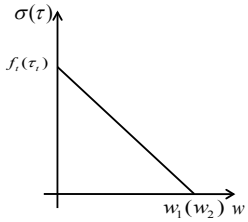

Figure 6: Linear decay cohesive law

where w is the crack opening displacement, $w_1(w_2)$ is the maximum width of the cracks. Introduce the fracture energy as an intrinsic property of concrete, and specify its formulation as

$$G_f = \int_0^{w_1} f dw \tag{53}$$

Apparently, for the $f-w$ diagram shown in Fig. 6, G_f can be expressed as

$$w_1 = 2G_f / f_t \tag{54}$$

As for the shear fracture (Model-Ⅱ fracture), the cohesive stress can be expressed as the function of crack shear displacement (Fig. 6). Then the shear fracture energy G_s is introduced for Model-Ⅱ fracture and the cohesive stress can be obtained as the Model-Ⅱ fracture.

5.2 Random field representation for fracture energy

Since the damage evolution is brought by the development of micro-cracks, the fracture energy is the primary parameter in the cracking process. Thus, the fracture energy is modeled as a random field to capture the heterogeneities of concrete.

In order to represent the random distribution of aggregates and mortar in concrete, a two-phase random field is generated by Hermite polynomial expansions [Ilango, Sarkar and Sameen (2013)], which transfers the original stochastic harmonic function [Chen, Sun, Li et al. (2013)] based Gaussian random field into two-phase random field. The fracture energy is chosen as the two-phase random field as

$$G_f(\boldsymbol{x}) = \begin{cases} A & \text{if } \boldsymbol{x} \text{ is in the strong phase (aggregate)} \\ B & \text{if } \boldsymbol{x} \text{ is in the weak phase (mortar)} \end{cases} \tag{55}$$

where $\boldsymbol{x}(x_1, x_2)$ is a 2-D vector which indicates the position; A and B are the value of fracture energy of aggregates and mortar, respectively.

Define the probability of strong phase as ρ, and the probability of weak phase can be easily calculate as $1-\rho$. From the above definition, we can see that strong phase of concrete has a probability equal to the ratio of aggregate as ρ, and weak phase has the a probability equal to the ratio of mortar as $(1-\rho)$.

$$R_{ZZ}(\xi_1, \xi_2) = \sigma^2 \exp\left(-\left(\frac{\xi_1}{b_1}\right)^2 - \left(\frac{\xi_2}{b_2}\right)^2\right), \quad -\infty < x_1 < \infty, -\infty < x_2 < \infty \tag{56}$$

where ξ_1, ξ_2 are the separation distances along the x_1 and x_2 directions respectively; and b_1 , b_2 are the correlation length with x_1 and x_2.

In the multi-scale analysis of this paper, the microscopic as well as the macroscopic parameters are from experimental results [Ren, Yang, Zhou et al. (2008)]. As for the random field of micro-cell, the ratio of the aggregate is ρ=0.451 , according to experimental mix proportion. The fracture energy of aggregates and mortar are $A = 180\text{N/mm}$ and $B = 60\text{N/mm}$. The correlation length is chosen as the maxim aggregate size with $b_1 = b_2 = 8\text{mm}$. By the aforementioned procedure, 100 samples are generated and 2 samples are given in Fig. 7.

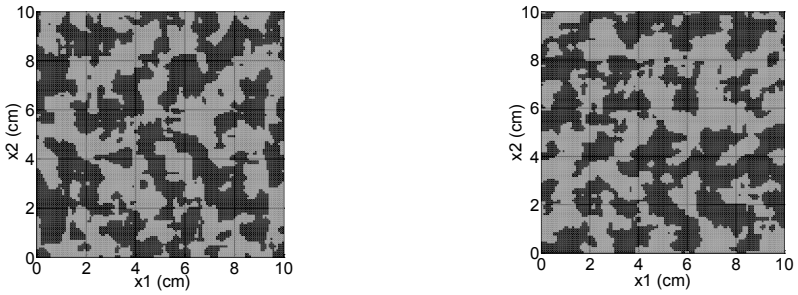

(a) sample 1 (b) sample 2

Figure 7: Random samples of fracture energy

5.3 Micro-cell simulation results

According to the test results, the material properties of Young's modulus and Poisson's ratio are E=37559MPa , ν=0.2 . The tensile strength of the matrix is $f_t = 3.25$MPa . The crack propagation in a micro-cell at different loading stages under uniaxial tension and pure shear are shown in Figs. 8 and 9, where ε_u denotes maximum strain.

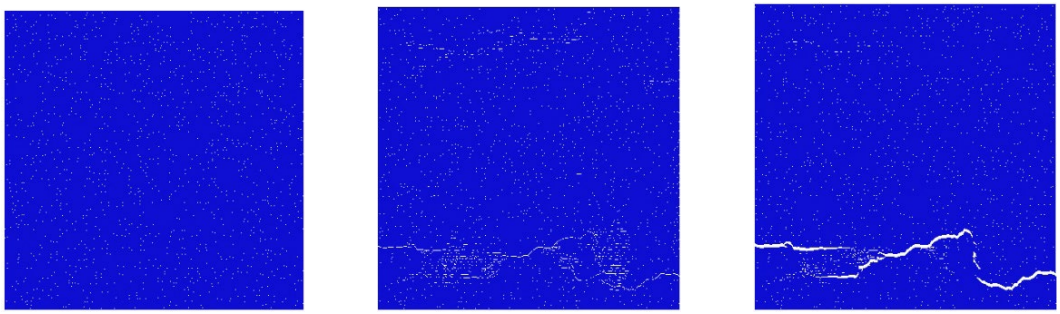

(a) ε=0.2ε_u (b) ε=0.7ε_u (c) ε=ε_u

Figure 8: Crack propagation of micro-cell under tensile test (Sample 23)

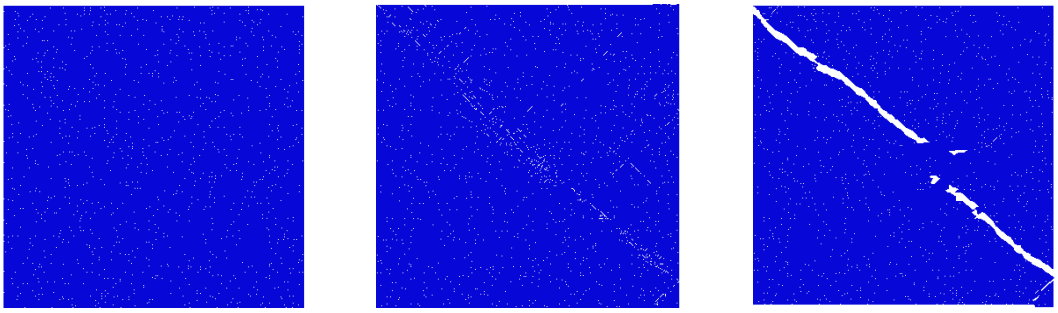

(a) ε=0.2ε_u (b) ε=0.7ε_u (c) ε=ε_u

Figure 9: Crack propagation of micro-cell under pure shear (Sample 23)

Then the homogenized stress-strain relationship and damage evolutions of each micro-cell can be obtained by Eqs. (33), (34), (37) and (38). The samples of tensile homogenized stress and mean value of damage variable are depicted in Fig. 10. Similarly, the samples of shear homogenized stress and damage variable are demonstrated in Fig. 11.

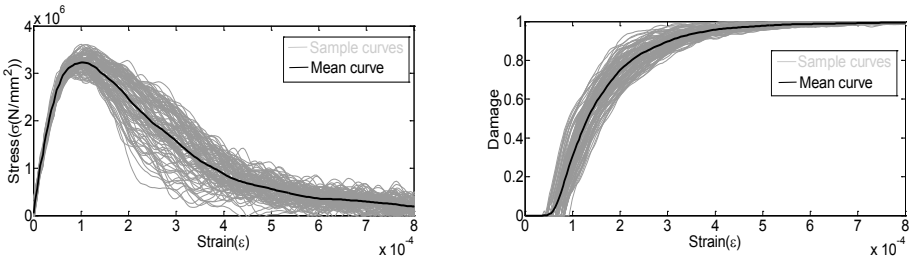

(a) homogenized stress-strain (b) tensile damage curves

Figure 10: Tensile homogenization results

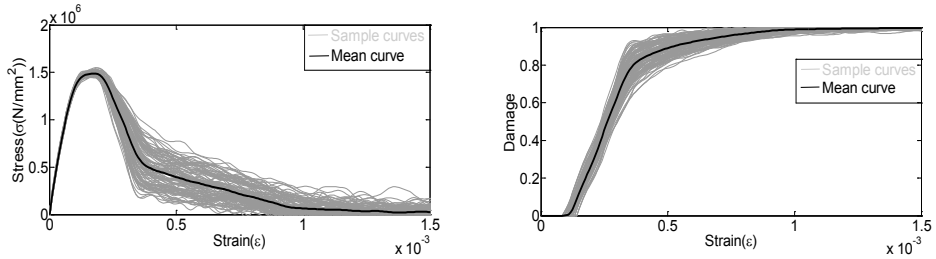

(a) homogenized stress-strain (b) shear damage curves

Figure 11: Shear homogenization results

6 Model verification

To illustrate the applicability and effectiveness of the proposed model, several numerical examples of various loading conditions of concrete are presented in this section.

6.1 Uniaxial test results

The experimental data for the high performance concrete [Ren, Yang, Zhou et al. (2008)] are used to calibrate the multi-scale damage model. The concrete samples, with the dimension of $150\,\text{mm}\times150\,\text{mm}\times50\,\text{mm}$, under uniaxial and biaxial loading are investigated in this paper. Since the CDM framework has been applied in the macro-scale analysis, the material involving in the simulation both for the uniaxial and biaxial tests are chosen based on the experimental identification as E=37559 MPa, ν=0.2, ϑ=1.16, ξ_p^+=0.2 and ξ_p^-=0.9. The mean curve of tensile and shear damage evolution in Section 6.1 is used in the uniaxial test, correspondingly. It is observed from Figs. 12 and 13, predictions from the numerical model agree well with the experimental data both for uniaxial tensile and compressive tests, especially for the post-peak nonlinear softening branches.

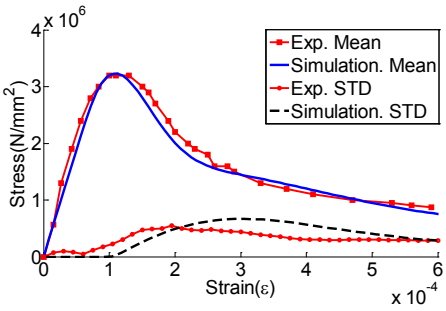

Figure 12: Uniaxial tensile test

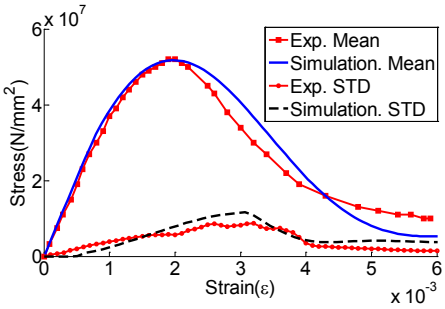

Figure 13: Uniaxial compressive test

6.2 Biaxial test results

The capacity to predict the multi-axial behavior of the multi-scale damage model is also verified by the biaxial compressive tests reported by Ren et al. [Ren, Yang, Zhou et al. (2008)]. In the biaxial compressive concrete simulation, the same material parameters are adopted as the uniaxial tests. Fig. 14 depict the both the experimental data and the numerical results for different strain ratio ($\varepsilon_2 / \varepsilon_1 = 0.1;\ 0.4;\ 1$).

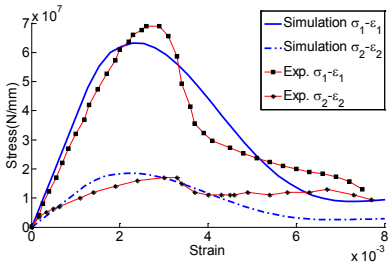

(a) Biaxial compressive test ($\varepsilon_2 / \varepsilon_1 = -0.1 / -1$)

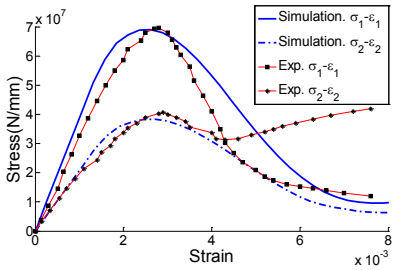

(b) Biaxial compressive test ($\varepsilon_2 / \varepsilon_1 = -0.4 / -1$)

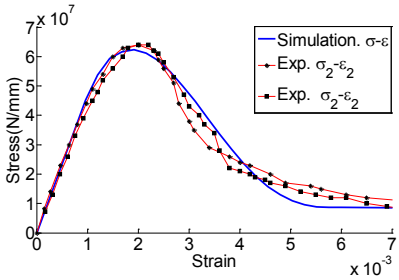

(c) Biaxial compressive test ($\varepsilon_2 / \varepsilon_1 = -1 / -1$)

Figure 14: Biaxial compressive tests

As shown in Fig. 14, the present multi-scale damage model can capture the stress-strain behavior of concrte when comparing with the experimental data under the primary loading direction. However, there exists a rehardening after the softenning stage under the secondary loading direction by the experimental observation in Fig. 14(b). To the best knowledge of the authors, this rehardening is possibily attributed to the complex combination of residual stress of the unloading stage and the shear dilation involving in the concrete. Since the physical priciple of the this rehardening is still unclear, some further studies should be carried from the micro-scale simulation to emplify the given multi-scale damge model.

6.3 Biaxial envelop

The data for the biaxial envelop is from the well-documented experimental results [Kupfer, Hilsdorf and Rusch (1969)]. Based on the aforementioned multi-scale simulation, the biaxial peak stress envelop can be simulated.

To illustrate the difference between the energy equivalent strain provided in this paper and the classical definition of equivalent strain, a similar but distinct equivalent strain notion from Mazars [Mazars (1986)] is given, herein. As for the bi-axial stress, the tensile and shear damage are intrigued by the tensile and compressive strain, respectively. Therefore, the equivalent $\hat{\varepsilon}^{e+}$ and $\hat{\varepsilon}^{e-}$ are given as

$$\hat{\varepsilon}^{e+} = \sqrt{\sum_{i=1}^{2} \left\langle \varepsilon_i^{e+} \right\rangle^2} \qquad \varepsilon_i^{e+} = \frac{\varepsilon_i^e + \left| \varepsilon_i^e \right|}{2} \tag{57}$$

$$\hat{\varepsilon}^{e-}=\sqrt{\sum_{i=1}^{2}\left(\varepsilon_i^{e-}\right)^2} \qquad \varepsilon_i^{e-}=\frac{\varepsilon_i^e-\left|\varepsilon_i^e\right|}{2} \tag{58}$$

where ε_i^e are the principle elastic strains.

The comparison between the experimental data and the simulation results is demonstrated in Fig. 15.

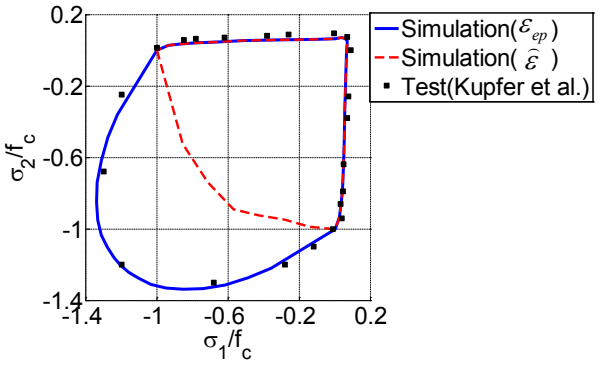

Figure 15: Biaxial peak stress envelop

It should be noted that the ratio between the tensile and compressive strength for the high performance concrete in this simulation is less than the ordinary concrete in the experiment. Therefore, the overall simulation results for biaxial envelop under the tensile-compressive loading and biaxial tensile loading is slightly less than the experimental results. However, the similar trends under the tensile-compressive loading and biaxial loading show the good agreement of the simulation results and experimental results. Meanwhile, as for the bi-compressive part, the agreement between the simulation and test results validate the multi-scale damage model. It is also demonstrated in Fig. 15 that the bi-compressive behavior of the concrete is well captured by using the energy equivalent strain when compare to the equivalent strain results.

6.4 Precast laminated concrete slab

In order to further apply the present multi-scale damage model to the structural analysis, the simulation of a precast laminated concrete slab is carried. The size of the precast laminated concrete slab is 6 m×6 m, and the thickness of both the precast and cast-in-situ layer is 80 mm. The set-up of the slab and arrangement of reinforcement are depicted in Figs. 16 and 17.

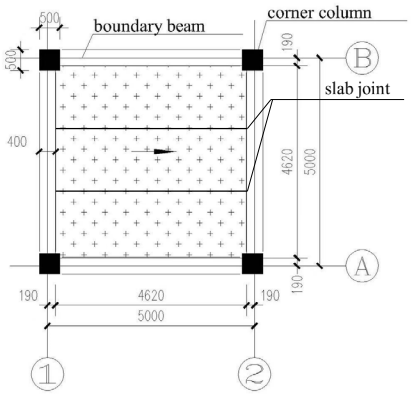

Figure 16: Precast laminated concrete slab

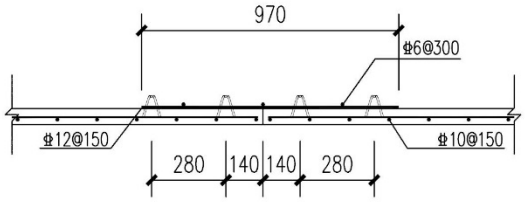

Figure 17: Reinforcement of the slab

Concrete and steel reinforcing bars are modelled by 3-D continuum elements and truss elements, respectively. The material behavior of concrete is described by the proposed multi-scale damage model, which has been implemented in ABAQUS by the user's subroutines. The material properties of concrete are chosen as the same in Section 6.1 where the damage curves are from the same micro-cell simulations for simplicity. And the non-linearity of steel is reproduced by the standard plastic model. The load-deflection curve is shown in Fig. 18. And Figs. 19 and 20 depict the stresses of both the concrete slab and rebars. The simulation results indicate good compatibility of the model into the structural analysis.

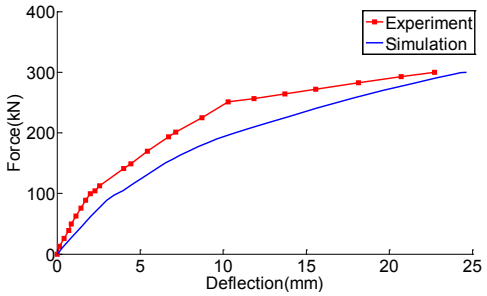

Figure 18: Load-deflection curve

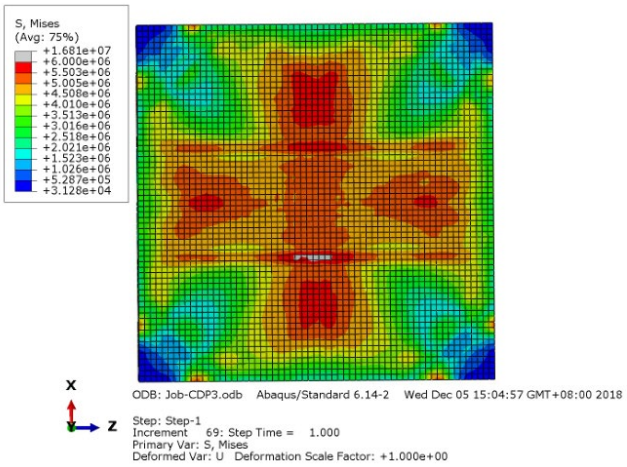

Figure 19: Stress of concrete slab

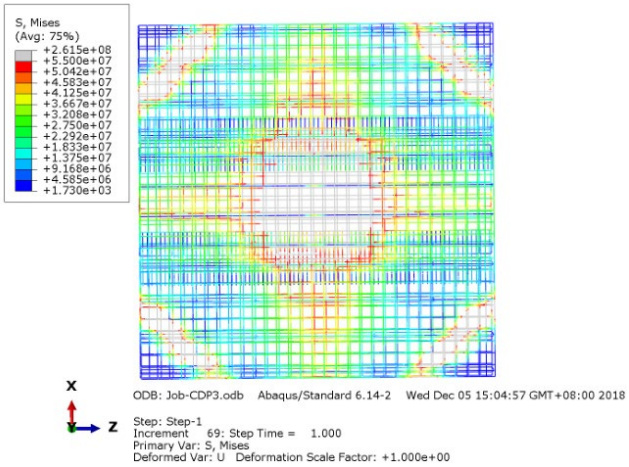

Figure 20: Stress of rebar

7 Conclusion

This manuscript is devoted to the presentation of a multi-scale damage model, mainly intended to expand it into two- or three-dimensional stress combinations. To this end, the CDM is firstly introduced as the framework of the multi-scale damage model to introduce the constitutive law and basic damage variables, the tensile and shear damage. As the bridge of cracked micro-structure and homogenized macro continua, the HFE between the macro-scale and micro-scale has been given. Then, the damage on the macro-scale can be represent as the function of homogenized HFE. Both the uniaxial tensile and shear damage evolution can be obtained by the micro-void cell analysis and multi-scale energy bridging equation. Stemming from the DERRs and damage consistent condition in CDM framework, the energy equivalent strain is introduced to link the uniaxial and multi-dimensional

damage law. As such, the damage model from the uniaxial stress state analysis can be expanded to the multi-dimensional stress state in the engineering application.

A series of numerical simulations have been presented that illustrate the qualitative agreement between multi-scale damage model and the experimental results of high-performance concrete. In particular, the biaxial compression and peak stress envelop of concrete is well captured by this model, whereas only uniaxial micro-cell analysis needs to be performed instead of the time consuming micro-cell analysis for each strain ratio to attain the damage evolution. An attractive feature of the present multi-scale damage is that it is straightforward to construct a multi-scale damage model from micro-structure of concrete, and is applicable handle the multi-dimensional complex problems in the concrete structural nonlinear analysis.

Acknowledgement: The support of this work by National Science Foundation of China under Grant No. 51808499 and Science Foundation of Zhejiang Province of China under the Grant No. LQ18E080009 and 2018C03033-2 is gratefully acknowledged. We would also like to express our sincere appreciations to the anonymous referee for valuable suggestions and corrections.

Conflicts of Interest: The authors declare that they have no conflicts of interest to report regarding the present study.

References

Bazant, Z. P.; Planas, J. (1997): *Fracture and Size Effect in Concrete and Other Quasibrittle Materials*, vol. 16. CRC Press.

Bosco, E.; Kouznetsova, V. G.; Geers, M. (2015): Multi-scale computational homogenization-localization for propagating discontinuities using X-FEM. *International Journal for Numerical Methods in Engineering*, vol. 102, no. 3-4, pp. 496-527.

Chen, J. B.; Sun, W. L.; Li, J.; Xu, J. (2013): Stochastic harmonic function representation of stochastic processes. *Journal of Applied Mechanics*, vol. 80, no. 1, pp. 1-11.

Dascalu, C.; Bilbie, G.; Agiasofitou, E. K. (2008): Damage and size effects in elastic solids: a homogenization approach. *International Journal of Solids and Structures*, vol. 45, no. 2, pp. 409-430.

Faria, R.; Oliver, J.; Cervera, M. (1998): A strain-based plastic viscous-damage model for massive concrete structures. *International Journal of Solids and Structures*, vol. 35, no. 14, pp. 1533-1558.

Feng, D.; Ren, X.; Li, J. (2018): Softened damage-plasticity model for analysis of cracked reinforced concrete structures. *Journal of Structural Engineering*, vol. 144, no. 6, 04018044.

Feng, D.; Li, J. (2015): Stochastic nonlinear behavior of reinforced concrete frames. II: Numerical simulation. *Journal of Structural Engineering*, vol. 142, no. 3, 04015163.

Fish, J.; Yu, Q.; Shek, K. (1999): Computational damage mechanics for composite materials based on mathematical homogenization. *International Journal for Numerical*

Methods in Engineering, vol. 45, no. 11, pp. 1657-1679.

Gross, D.; Seelig, T. (2011): *Fracture Mechanics: with an Introduction to Micromechanics*. Springer Science & Business Media.

Hill, R. (1984): On macroscopic effects of heterogeneity in elastoplastic media at finite strain. *Mathematical Proceedings of the Cambridge Philosophical Society*. Cambridge University Press.

Ilango, S. J. J.; Sarkar, S.; Sameen, A. (2013): Reconstruction of 2-D porous media using Karhunen-Lóeve expansion. *Probabilistic Engineering Mechanics*, vol. 32, no. 1, pp. 56-65.

Ju, J. W. (1989): On energy-based coupled elastoplastic damage theories: constitutive modeling and computational aspects. *International Journal of Solids and structures*, vol. 25, no. 7, pp. 803-833.

Krajcinovic, D.; Silva, M. A. G. (1982): Statistical aspects of the continuous damage theory. *International Journal of Solids and Structures*, vol. 18, no. 7, pp. 551-562.

Kupfer, H.; Hilsdorf, H. K.; Rusch, H. (1969): Behavior of concrete under biaxial stresses. *Journal Proceedings*, vol. 66, no. 2, pp. 656-666.

Li, J.; Ren, X. (2009): Stochastic damage model for concrete based on energy equivalent strain. *International Journal of Solids and Structures*, vol. 46, no. 11, pp. 2407-2419.

Li, W.; Siegmund, T. (2004): Numerical study of indentation delamination of strongly bonded films by use of a cohesive zone model. *Computer Modeling in Engineering & Sciences*, vol. 5, no. 1, pp. 81-90.

Liang, S.; Chen, J.; Li, J.; Lin, S.; Chi, S. et al. (2017): Numerical investigation of statistical variation of concrete damage properties between scales. *International Journal of Fracture*, vol. 208, no. 12, pp. 97-113.

Liang, S.; Ren, X.; Li, J. (2018): A mesh-size-objective modeling of quasi-brittle material using micro-cell informed damage law. *International Journal of Damage Mechanics*, vol. 27, no. 6, pp. 1249-1257.

Lin, S.; Chen, J.; Liang, S. (2016): A damage analysis for brittle materials using stochastic micro-structural information. *Computational Mechanics*, vol. 57, no. 3, pp. 371-385.

Lubliner, J. (1972): On the thermodynamic foundations of non-linear solid mechanics. *International Journal of Non-Linear Mechanics*, vol. 7, no. 3, pp. 237-254.

Mazars, J. (1986): A description of micro-and macroscale damage of concrete structures. *Engineering Fracture Mechanics*, vol. 25, no. 5, pp. 729-737.

Mazars, J.; Pijaudier-Cabot, G. (1989): Continuum damage theory-application to concrete. *Journal of Engineering Mechanics*, vol. 115, no. 2, pp. 345-365.

Ortiz, M. (1985): A constitutive theory for the inelastic behavior of concrete. *Mechanics of Materials*, vol. 4, no. 1, pp. 67-93.

Ostoja-Starzewski, M. (2006): Material spatial randomness: from statistical to representative volume element. *Probabilistic Engineering Mechanics*, vol. 21, no. 2, pp. 112-132.

Ren, X.; Chen, J.; Li, J.; Slawson, T. R.; Roth, M. J. (2011): Micro-cracks informed damage models for brittle solids. *International Journal of Solids and Structures*, vol. 48, no. 10, pp. 1560-1571.

Ren, X.; Li, J. (2012): Dynamic fracture in irregularly structured systems. *Physical Review E*, vol. 85, no. 5, 055102.

Ren, X. D.; Yang, W. Z.; Zhou, Y.; Li, J. (2008): Behavior of high-performance concrete under uniaxial and biaxial loading. *ACI Materials Journal*, vol. 105, no. 6, pp. 548-557.

Resende, L. (1987): A damage mechanics constitutive theory for the inelastic behaviour of concrete. *Computer Methods in Applied Mechanics and Engineering*, vol. 60, no. 1, pp. 57-93.

Simo, J. C.; Ju, J. W. (1987): Strain-and stress-based continuum damage models-I. Formulation. *International Journal of Solids and Structures*, vol. 23, no. 7, pp. 821-840.

Sun, B.; Li, Z. (2015): Adaptive image-based method for integrated multi-scale modeling of damage evolution in heterogeneous concrete. *Computers & Structures*, vol. 152, no. 6, pp. 66-81.

Wu, J. Y.; Li, J.; Faria, R. (2006): An energy release rate-based plastic-damage model for concrete. *International Journal of Solids and Structures*, vol. 43, no. 3, 583612.

Appendix A.

With the consideration of the equilibrium equation given in Eq. (25), the averaged Helmholtz free energy can be written as

$$\begin{aligned}\int_{\Omega_y}\psi^{\lambda}d\Omega &= \frac{1}{2}\int_{\Omega_y}\boldsymbol{\sigma}^{\lambda}:\varepsilon^{\lambda}d\Omega \\ &= \frac{1}{2}\int_{\Omega_y}\frac{1}{2}\boldsymbol{\sigma}^{\lambda}:\left(\nabla\otimes\boldsymbol{u}^{\lambda}+\boldsymbol{u}^{\lambda}\otimes\nabla\right)d\Omega \\ &= \frac{1}{2}\int_{\Omega_y}\frac{1}{2}\left[\nabla\cdot\left(\boldsymbol{u}^{\lambda}\cdot\boldsymbol{\sigma}^{\lambda}\right)+\nabla\cdot\left(\boldsymbol{\sigma}^{\lambda}\cdot\boldsymbol{u}^{\lambda}\right)-\boldsymbol{u}^{\lambda}\cdot\nabla\cdot\boldsymbol{\sigma}^{\lambda}-\nabla\cdot\boldsymbol{\sigma}^{\lambda}\cdot\boldsymbol{u}^{\lambda}\right]d\Omega \\ &= \frac{1}{2}\int_{\Omega_y}\nabla\cdot\left(\boldsymbol{u}^{\lambda}\cdot\boldsymbol{\sigma}^{\lambda}\right)d\Omega\end{aligned} \tag{59}$$

By using the divergence theorem [Ren, Chen, Li et al. (2011)], Eq. (59) becomes

$$\begin{aligned}\int_{\Omega_y}\psi^{\lambda}d\Omega &= \frac{1}{2}\int_{\Omega_y}\nabla\cdot\left(\boldsymbol{u}^{\lambda}\cdot\boldsymbol{\sigma}^{\lambda}\right)d\Omega \\ &= \frac{1}{2}\oint_{\partial\Omega_y}\boldsymbol{u}^{\lambda}\cdot\boldsymbol{\sigma}^{\lambda}\cdot\boldsymbol{n}d\Omega-\frac{1}{2}\oint_{\Gamma_c}\boldsymbol{u}^{\lambda}\cdot\boldsymbol{\sigma}^{\lambda}\cdot\boldsymbol{n}d\Omega \\ &= \frac{1}{2}\oint_{\partial\Omega_y}\boldsymbol{u}^{\lambda}\cdot\boldsymbol{t}^{\lambda}d\Omega-\frac{1}{2}\oint_{\Gamma_c}\boldsymbol{u}^{\lambda}\cdot\boldsymbol{h}d\Omega\end{aligned} \tag{60}$$

In seeking the relationship of the HFE between the macro-continuum and micro-cell, a linear essential boundary condition, which serves as a standard procedure in homogenization [Gross and Seelig (2011)], is applied to the entire boundary of the elastic microscopic cell

$$\boldsymbol{u}^{\lambda} = \boldsymbol{\varepsilon} \cdot \boldsymbol{x} \text{ on } \partial\Omega_y \tag{61}$$

Then, substitute Eq. (61) into the first term on the right hand side of Eq. (60) as

$$\begin{aligned} \frac{1}{2}\oint_{\partial\Omega_y} \boldsymbol{u}^{\lambda} \cdot \boldsymbol{t}^{\lambda} d\Omega &= \frac{1}{2}\oint_{\partial\Omega_y} (\boldsymbol{\varepsilon} \cdot \boldsymbol{x}) \cdot \boldsymbol{t}^{\lambda} d\Omega \\ &= \frac{1}{2}\oint_{\partial\Omega_y} \boldsymbol{t}^{\lambda} \otimes \boldsymbol{x} d\Omega : \boldsymbol{\varepsilon} \\ &= \frac{1}{2} V_y \boldsymbol{\sigma} : \boldsymbol{\varepsilon} \\ &= V_y \psi^e \end{aligned} \tag{62}$$

Incorporating both Eqs. (59) and (62), the multi-scale energy bridging can be attained as follows

$$\psi^e = \frac{1}{V_y}\left(\int_{\Omega_y} \psi^{\lambda} \mathrm{d}\Omega + \frac{1}{2}\oint_{\Gamma_c} \boldsymbol{u}^{\lambda} \cdot \boldsymbol{h} \mathrm{d}\Gamma \right) \tag{63}$$